Etrinabdione (VCE-004.8), a B55α activator, promotes angiogenesis and arteriogenesis in critical limb ischemia.

Adela García-Martín, PhD[1,2,3], María E. Prados, PhD[1,2,3], Isabel Lastres-Cubillo [1,3], Francisco J. Ponce-Diaz-Martín[1,2,3], Laura Cerero[1,2,3], Martin Garrido-Rodríguez, PhD[4], Carmen Navarrete, PhD[1,3], Rafael Pineda, PhD [1,2,3], Ana B. Rodríguez [1,2,3], Ignacio Muñoz, MD, PhD[1,3], Javier Moya[1,3], Antonella Medeot[1,3], José A. Moreno[1,3], Antonio Chacón, MD, PhD[1,3]. José García-Revillo, MD, PhD[1,3] and Eduardo Muñoz, MD, PhD[1,2,3]

[1] Maimonides Biomedical Research Institute of Córdoba (IMIBIC), Córdoba, Spain.
[2] Cellular Biology, Physiology and Immunology Department, University of Córdoba, Spain.
[3] Hospital Universitario Reina Sofía, Córdoba, Spain.
[4] Heidelberg University, Faculty of Medicine, and Heidelberg University Hospital, Institute for Computational Biomedicine, Bioquant, Heidelberg, Germany.

Short title: Etrinabdione and peripheral artery disease

Corresponding author: Eduardo Muñoz. Maimonides Biomedical Research Institute of Córdoba, University of Córdoba, Avda Menéndez Pidal s/n. 14004. Córdoba, Spain. Phone: +34 677 437513. Email: fi1muble@uco.es

ABSTRACT

Background: Vasculogenic therapies explored for the treatment of peripheral artery disease (PAD) have encountered minimal success in clinical trials. Addressing this, B55α, an isoform of protein phosphatase 2A (PP2A), emerges as pivotal in vessel remodeling through activation of hypoxia-inducible factor 1α (HIF-1α). This study delves into the pharmacological profile of VCE-004.8 (Etrinabdione) and evaluates its efficacy in a preclinical model of critical limb ischemia, with a focus on its potential as a PP2A/B55α activator to induce angiogenesis and arteriogenesis.

Methods: Vascular endothelial cells were used for *in vitro* experiments. Aorta ring assay was performed to explore sprouting activity. Matrigel plug-in assay was used to assess the angiogenic potential. Critical limb ischemia (CLI) in mice was induced by double ligation in the femoral arteria. Endothelial vascular and fibrotic biomarkers were studied by immunohistochemistry and qPCR. Arteriogenesis was investigated by microvascular casting and micro-CT. Proteomic analysis in vascular tissues was analyzed by LC-MS/MS. *Ex-vivo* expression of B55α and biomarkers were investigated in artery samples from PAD patients.

Results: VCE-004.8 exhibited the ability to induce B55α expression and activate the intersecting pathways B55α/AMPK/Sirtuin 1/eNOS and B55α/PHD2/HIF-1α. VCE-004.8 prevented OxLDL and H_2O_2-induced cytotoxicity, senescence, and inflammation in endothelial cells. Oral VCE-004.8 increased aorta sprouting *in vitro* and angiogenesis *in vivo*. In CLI mice VCE-004.8 improved collateral vessel formation and induced endothelial cells proliferation, angiogenic gene expression and prevented fibrosis. The expression of B55α, Caveolin 1 and Sirtuin-1 is reduced in arteries from CLI mice and PAD patient, and the expression of these markers was restored in mice treated with VCE-004.8.

Conclusions: The findings presented in this study indicate that Etrinabdione holds promise in mitigating endothelial cell damage and senescence, while concurrently fostering arteriogenesis and angiogenesis. These observations position Etrinabdione as a compelling candidate for the treatment of PAD, and potentially other cardiovascular disorders.

Keywords: Etrinabdione, VCE-004.8, PPA2/B55α, HIF-1α, Sirtuin 1, eNOS, angiogenesis.

Novelty and Significance

What Is Known?

- The phosphatase PPA2/B55α stabilizes endothelial cells (ECs) in response to cell stress conditions, thereby protecting ECs from apoptosis and promoting angiogenesis.
- Etrinabdione (VCE-004.8) functions as a potent activator of PPA2/B55α inducing PHD2 dephosphorylation at ser125 and fostering HIF activation.
- VCE-004.8 prevents vascular damage in preclinical models of systemic and cardiac fibrosis and alleviates blood-brain barrier disruption in neuroinflammatory conditions.
- VCE-004.8 is also a dual agonist of PPARγ and CB_2 receptors and shows antiinflammatory activity.
- Oral VCE-004.8 has meet the primary endpoints of safety and tolerability in a Phase IIa clinical trial with systemic sclerosis patients (clinicaltrial.gov: NCT03745001).

What New Information Does This Article Contribute?

- Etrinabdione induces HIF-1α expression in endothelial cells through a novel pathway that potentially involves two axes: B55α/PHD2 and B55α/AMPK/Sirt1 signaling that may converge on HIF stabilization.
- Etrinabdione prevented endothelial cell damage and senescence, while inducing arteriogenesis and angiogenesis in CLI mice.
- In arteries of patients with PAD and in CLI mouse models, the expression levels of B55α, Caveolin 1, and Sirtuin 1 are diminished. However, treatment with Etrinabdione specifically in CLI mice prompts an increase in the levels of these proteins.
- Etrinabdione triggers neovascularization and angiogenesis specifically within hypoxic tissue in a critical ischemia model, with no impact on healthy tissue.

INTRODUCTION

Peripheral arterial disease (PAD) is one of the major leading cause of atherosclerotic cardiovascular morbidity[1]. Experimental approaches to the treatment of PAD have included the use of angiogenic factors as a recombinant protein or as gene therapy as well as stem cell therapy[2] but, neither of these strategies achieved significant benefits in clinical trials. Hence, there is an urgent demand for novel pharmacological targets and therapies capable of preventing endothelial damage and promoting angiogenesis and arteriogenesis to enhance blood flow in extremities.

The protein phosphatase 2A (PP2A) belong to a family of serine-threonine phosphatases, which are formed by a catalytic C subunit, a scaffold A subunit, and a regulatory B subunit, which confers specificity of PP2A for selective proteins substrates[3]. B55α (PPP2R2A) is one of the regulatory subunits that has been shown to directly dephosphorylates prolyl hydroxylase 2 (PHD2) on Ser125, resulting in a further reduction of its activity that ultimately stabilized and accumulated the hypoxia inducing factor 1α (HIF-1α)[4]. HIF-1, a heterodimeric basic-helix-loop-helix-paste protein that responds to oxygen tension, is activated by severe and mild hypoxia. Under hypoxic conditions, HIF-1α accumulates in the nucleus and dimerizes with HIF-1β to activate a plethora of genes including angiogenic factors such as vascular endothelial growth factor (VEGF), fibroblast growth factor (FGF) and angiopoietin, as well as an important number of genes involved in vascular and tissue remodeling.[5,6] HIF-1α is also activated by therapeutic preconditioning hypoxia and by hypoxia mimetic small compounds.[7,8] More recently, it has been shown that B55α stabilizes endothelial cells (ECs) in response to cell stress conditions, thereby protecting ECs from apoptosis and promoting angiogenesis. Thus, PP2A/B55α activators represent a new class of hypoxia mimetic compounds with potential in vessel remodeling, angiogenesis and endothelial cell protection[9].

The histone deacetylase Sirtuin 1 (Sirt1) belong to the family of Sirtuins, which are nicotinamide adenine dinucleotide (NAD^+)-dependent enzymes with multiple metabolic functions. The expression of Sirt1 is reduced with aging both in animal models and in humans, and a reduced expression is thought to be involved in age-related cardiovascular diseases. Indeed, Sirt1, which is activated by AMPK, is a critical modulator of the vascular function[10] and endothelial senescence is regarded as a prominent precursor of cardiovascular diseases including PAD and critical limb ischemia (CLI).[11] The key role of Sirt1 in the regulation of vascular homeostasis is mediated

through complex cellular mechanisms involved in the promotion of vasodilatory and regenerative functions at ECs, endothelial progenitor cells, and smooth muscle cells (SMC) levels.[12]

We have recently identified the cannabidiol aminoquinone VCE-004.8 (also known as Etrinabdione and EHP-101), as a PP2A/B55α activator that induces HIF-1α and HIF-2α stabilization.[13] In addition, VCE-004.8 is a dual activator of peroxisome proliferator-activated receptor-γ (PPARγ) and cannabinoid type 2 receptors (CB_2R).[14] VCE-004.8 showed efficacy in preclinical models of traumatic brain injury,[15] multiple sclerosis[13], bleomycin- and angiotensin-induced models of dermal, lung, cardiac, and kidney fibrosis[14, 16], metabolic syndrome[17] and stroke[18].

Etrinabdione (VCE-004.8) has finalized the stage 1 of a clinical Phase IIa trial in Systemic Sclerosis patients (Clinical Trials.gov: NCT04166552), and it had acceptable safety profile and was well-tolerated. Herein we have further investigated additional pharmacological attributes of VCE-004.8 and explored its efficacy in a model of CLI.

METHODS

Please see the Supplemental Material for detailed methods on cell cultures, transient transfections and luciferase assays, western blot analysis, measurement of NO (nitric oxide), Sirtuin 1 activity, NAD^+ /NADH ratio, senescence assay, aortic ring assay, *in vivo* angiogenesis, in *vivo* perfusion fixation and tissue processing procedures, confocal immunofluorescence microscopy, qPCR, and proteomic analysis). All experimental protocols followed the guidelines of animal care set by the EU guidelines 86/609/EEC, the Ethic Committee on Animal Experimentation at the University of Córdoba (Spain) and the Andalusian Regional Committee for Animal Experimentation approved all the procedures described in this study (31/03/2022/057). Human biopsies from patients were obtained by the Cardiovascular Surgery Unit of Hospital Universitario Reina Sofia of Cordoba, Spain (RSUH) and the protocol approved from the Ethics Committee of RSUH (reference: HIP-CI:1.0-01/06/2023).

Data Availability. The data that support the findings of this study are available from the corresponding author upon request.

161 **Test compound.** VCE-004.8 (also called Etrinabdione and EHP-101) [(1′R,6′R)−3-
162 (Benzylamine)−6-hydroxy-3′-methyl-4-pentyl-6′-(prop-1-en-2-yl) [1,1′bi(cyclohexane)
163]− 2′,3,6-triene-2,5-dione)] was produced under GMP conditions and provided by
164 VivaCell Biotechnology España, Spain). For animal use VCE-004.8 was dissolved in
165 sesame oil/Maisine CC® (50%/50%) and applied by oral gavage.
166
167 **Critical limb ischemia (CLI) mouse model**. Male C57BL/6 mice aged 10-12 weeks
168 were divided into 2 groups (CLI group and sham group). In the CLI group the femoral
169 artery and its side branches were double ligated with 6–0 silk sutures immediately distal
170 to the inguinal ligament and proximal to the popliteal bifurcation. Femoral nerves were
171 carefully preserved. The wound was irrigated with sterile saline and then the overlying
172 skin was closed using 4–0 vicryl sutures. Post-operative pain was reduced using
173 Lignocaine. A similar surgery without ligation of the femoral artery was performed on
174 the sham controls. The CLI group was administered VCE-004.8 (20 mg/kg) by oral
175 gavage every day until the end of the study and the sham control group was treated with
176 vehicle (Corn oil/Maisine® CC (50/50 (v/v)). At 10 and 28 days after ligation, the whole
177 limb and muscles were harvested for study.
178
179 **Vascular casting.** Mice were anesthetized and injected 1000 UI of heparin (i.p.). After
180 10 min, the mice were euthanized, the thorax was opened, and the aorta exposed. A
181 catheter was inserted into the descending aorta and fixed with sutures. Then mice were
182 perfused with PBS (37 °C, 80 ml) containing heparin, nitroglycerin, adenosine and
183 sodium nitroprusside to remove the blood and enhanced the vasodilatation of the vessels.
184 Microfil (MV-112 [white]; Flow Tech Inc, South Windsor, CT, USA) was perfused and
185 then filled the entire vascular bed. The Microfil polymerized overnight at 4°C, and the
186 samples were harvested and clarified in graded glycerol solutions (40%–100% glycerol
187 in water; glycerol increased by 20% at 24-hour intervals). The clarified specimens were
188 viewed on a dissecting microscope and Microfil retained in the vasculature was
189 investigated by μ-CT (X-ray tomography).
190
191 **Image acquisition μ-CT.** After Microfilm polymerization, the animals were hold inside
192 a Bruker SkyScan 1172 high resolution microtomography machine (Bruker micro-CT,
193 Kontich, Belgium). The X-ray source was set to a voltage of 50 kV and a current of 498
194 μA with a 0.5-mm Al filter in the beam path with an angular increment of 0.3°. Data were

195 transferred to a computer with NRecon, CTAn, CT Vol software, (Bruker), ImageJ
196 (http://rsb.info.nih.gov/ij/) and 3DSlicer v.3.4.0 open-source software
197 (https://pubmed.ncbi.nlm.nih.gov/22770690/) was using to analyze vessel numbers,
198 diameter, area, and volume, as well as arterial density.
199
200 **Laser capture microdissection (LCM) targeted mass spectroscopy.** LCM and
201 subsequent molecular analysis were carried out on slides immuno-stained using anti-α-
202 Smooth Muscle Actin (α-SMA) antibody of gastrocnemius muscles frozen sections. The
203 vessel marked with immunofluorescence α-SMA were dissected with ZEISS PALM
204 Microbeam micro dissected and collected for mass spectroscopy analysis.
205
206 **Proteomics data analysis.** To generate Figure 7B, we employed the log transformed
207 intensities for proteins annotated with the Gene Ontology term 'Angiogenesis' (GO:
208 0001525). The mass spectrometry proteomics data have been deposited to the
209 ProteomeXchange Consortium via the PRIDE partner repository with the dataset
210 identifier PXD050360.
211
212 **Statistical Analysis.** Data were expressed as the mean ± SEM or SD. One-way analysis
213 of variance (ANOVA) followed by the Tukey´s post-hoc test for parametric analysis or
214 Kruskal-Wallis post-hoc test in the case of non-parametric analysis tests will be used to
215 determine the statistical significance. The level of significance will be set at $p < 0.05$.
216 Statistical analyses will be performed using GraphPad Prism version 9 (GraphPad, San
217 Diego, CA, USA).
218
219 **RESULTS**
220
221 **VCE-004.8 induces B55α/PP2A in endothelial vascular cells.** We have demonstrated
222 that VCE-004.8, a hypoxia-mimetic cannabidiol aminoquinone derivative,
223 dephosphorylates PHD2 at ser-125 via a PP2A/B55α-dependent pathway, leading to the
224 induction of HIF-1α expression[13]. In this study, we further reveal that B55α expression in
225 EA-hy926 cells is primarily localized perinuclearly and is significantly upregulated
226 following exposure to VCE-004.8 (Fig. 1A). As anticipated, silencing B55α expression
227 with siRNA in EA-hy926 cells abrogated the VCE-004.8-induced stabilization of HIF-1α
228 (Fig. 1B). To investigate the functional impact of VCE-004.8 and HIF-1α on cell viability,

229 we subjected the cells to H_2O_2 treatment in the presence or absence of the compound.
230 VCE-004.8 greatly prevented H_2O_2-cytotoxicity in a concentration-dependent manner
231 (Fig. 1C), which was significantly counteracted by YC-1, a HIF-1α inhibitor (Fig. 1D).
232 Moreover, the cytoprotective effect of VCE-004.8 was evident in cells exposed to both
233 high glucose and OxLDL (Fig. 1S). Subsequently, to explore the anti-inflammatory
234 properties of VCE-004.8, EA-hy926 cells were incubated with proinflammatory
235 cytokines, and the expression of various markers was analyzed via confocal microscopy.
236 VCE-004.8 attenuated IL-1β+TNFα-induced VCAM-1 expression and restored the
237 expression of tight-junction proteins ZO-1 and CLD1 in IL-6/TNFα-treated cells.
238 Notably, tight-junction proteins play a crucial role in maintaining the integrity of vascular
239 endothelial cells[19]. Furthermore, VCE-004.8 also induced the expression of B55α under
240 inflammatory conditions (Fig. 2S).
241
242 **VCE-004.8 activates AMPK/Sirtuin-1 and prevents senescence in endothelial**
243 **vascular cells.** The protective role of the AMP-activated Protein Kinase (AMPK)
244 pathway, a pivotal cellular energy sensor, extends beyond metabolic homeostasis to
245 encompass cardiovascular protection. Vascular AMPK plays a crucial role in regulating
246 endothelial function, redox homeostasis, and inflammation.[20] Moreover, emerging
247 evidence indicates a functional interplay between AMPK and HIF pathways, contributing
248 to cellular survival adaptation[21]. Thus, we interrogated the participation of AMPK on the
249 pathways activated by VCE-004.8 in endothelial cells. VCE-004.8 induced AMPK
250 phosphorylation and upregulated the expression of Sirt1 and nicotinamide
251 phosphoribosyl transferase (NAMPT), also known as Visfatin, in EA.hy926 cells (Fig.
252 2A and 2B). A connection between AMPK and Sirt1 has been proposed since AMPK
253 activates Sirt1 through an increase in cellular NAD^+ level [22], while Sirt1 deacetylates the
254 AMPK kinase LKB1, leading to phosphorylation and activation of AMPK[23]. We found
255 that VCE-004.8 increases the enzymatic activity of Sirt1 and the NAD^+/NADPH ratio in
256 EA-hy926 cells (Fig. 2C and D). Moreover, silencing Sirt1 expression with siRNA
257 prevented the induction of HIF-1α expression by VCE-004.8 (Fig. S3A). To further
258 explore the effect of VCE-004.8 on cellular senescence EA.hy926 cells were treated with
259 H_2O_2 and the expression of both SA-β-gal^+ cells, Sirt1 and p21 proteins analyzed. VCE-
260 004.8 significantly inhibited H_2O_2-induced senescence and p21 expression and restored
261 the expression of Sirt1 that was downregulated with the H_2O_2 treatment (Fig. 2E and 2F).
262 In addition, pretreatment with dorsomorphin (DS), an AMPK inhibitor, or EX527, a Sirt1

263 inhibitor, separately or in combination, also inhibited both VCE-004.8-induced EPO-Luc,
264 serving as a surrogated marker of HIF activation (Fig. S3B), and H_2O_2-induced
265 cytotoxicity (Fig. S3C). We also investigated eNOS phosphorylation at ser1177, another
266 target of AMPK, and observed that VCE-004.8 induced eNOS phosphorylation (Fig. 3A)
267 as well as NO production (Fig. 3B) in EA.hy926 cells. Interestingly, eNOS
268 phosphorylation was significantly diminished in B55α siRNA cells, providing further
269 evidence for the functional interaction between B55α and AMPK in response to VCE-
270 004.8. Taken together, these findings suggest that in addition to PHD2/HIF-1α activation,
271 the AMPK/Sirt1/eNOS signaling pathways play a significant role in the mechanism of
272 action of VCE-004.8.
273
274 **Angiogenic and arteriogenic effects of VCE-004.8.** Vascular regeneration,
275 angiogenesis, arteriogenesis and vasculogenesis are the main objectives for potential
276 vasculogenic therapies for PAD[24]. To evaluate the effect of VCE-004.8 in vascularization
277 and sprouting, we performed an *ex vivo* aortic ring assay. We found that VCE-004.8, as
278 well as VEGF and dimethyloxallyl glycine (DMOG), an enzymatic Pan-PHD inhibitor,
279 induced vascularization *in vitro*, indicated by the formation of new sprouts as well as
280 sprout area (Fig. S4A). Next, to investigate the angiogenic potential of VCE-004.8 in
281 vivo, we conducted a Matrigel plug *in situ* assay. After ten days following the
282 subcutaneous injection of Matrigel into the flank, no signs of angiogenesis were observed
283 in the negative control group (without treatment), in contrast to Matrigel embedded with
284 VEGF (positive control). Oral treatment with VCE-004.8 (10 and 20 mg/kg) clearly
285 increased the formation of functional vessel identified by $CD31^+/\alpha SMA^+$ staining and the
286 proliferative activity of vascular endothelial cells were identified by expression of
287 $CD31^+/Ki67^+$ cells. Moreover, we also confirmed that B55α is also expressed in the new
288 formed vessels (Fig. S4B).
289 To further explore the effect of VCE-004.8 in a model of critical limb ischemia
290 (CLI) a doble ligation in the femoral arteria was performed in mice and 24 h later animals
291 were treated daily with oral VCE-004.8. After 10 or 28 days of treatment the effect of
292 VCE-004.8 on collateral vessels was investigated by vascular casting and microcomputed
293 tomography (μ-CT) imaging. It is shown in Figure 4A that treatment with VCE-004.8
294 clearly induced collateral artery formation in the ligated limb compared to the non-ligated
295 control limb, which was not affected by the treatment. These results are in good

296 correlation with the mRNA expression of *Hif1α* and the HIF-regulated proangiogenic
297 genes *Vegfa*, *Epo* and *Hgf* in the gastrocnemius muscle in the affected limb but not in
298 control limb (Fig. 4B) suggesting that the effect of VCE-004.8 is specific to damaged
299 tissues.
300
301 **Angiogenic and antifibrotic effects of VCE-004.8 in CLI mice.** Reperfusion of
302 ischemic tissues depends on angiogenesis that is required for a proper tissue blood flow[25,
303 26]. Thus, we explored the effect of VCE-004.8 on angiogenesis and vascular density in
304 the gastrocnemius tissue. VCE-004.8 induced angiogenesis measured by the number of
305 vessels ($CD31^+/\alpha SMA^+$) and lumen perimeter vessel per area in the ligated limb without
306 affecting the contralateral limb (Fig. 5A). We also investigated endothelial cells
307 proliferation, a key event in angiogenesis, and found that VCE-004.8 significantly
308 induced cell proliferation as measured by CD31/Ki67 co-staining (Fig. 5B). CD34 is one
309 of the surface markers for endothelial progenitor cells, which plays a major role in
310 angiogenic and vasculogenic activities during neovascularization[27]. Indeed, $CD34^+$ cells
311 isolated from peripheral blood have been widely used in experimental therapies including
312 cardiovascular diseases and critical leg ischemia[28, 29]. VCE-004.8 treatment significantly
313 increased the average the of number of $CD34^+/CD31^+$ as well as $CD34^+/CD31^-$ cells in
314 the ligated limb compared with the contralateral limb (Fig. 6A).
315 Evidence supports the involvement of fibrosis in the pathophysiology of PAD[30].
316 Fibrosis is associated with various pathological processes in vascular tissues and may
317 contribute to the progression of PAD[31]. Herein, we investigated the expression of
318 Tenascin C (TNC), a marker for fibrosis in both CLI mice and in ex-vivo human samples
319 from PAD patients [32]. TNC expression was detected in the ligated limb of CLI mice (Fig.
320 6B) and human aorta from PAD patients (Fig. 6C) and treatment with VCE-004.8
321 significantly alleviated TNC deposition in the ischemic tissue relative to the contralateral
322 leg (Fig. 6B).
323
324 **B55α and Sirtuin 1 expression in CLI mice and human arteries.** As demonstrated
325 above, our data revealed a mechanistic link between B55α and Sirt1 expression and
326 activity in vitro. Consequently, we investigated the expression of both proteins in tissues.
327 B55α and Sirt1 expression were found to be downregulated in the ligated limb from CLI
328 mice compared to the contralateral limb (Fig. 7A and 7B), and similar results were

329 observed in the aorta from PAD patients (diseased) compared to healthy tissues (Fig. 7D).
330 VCE-004.8 treatment completely restored the expression of both proteins in the ligated
331 limb of CLI mice. The mRNA expression levels of B55α and Sirt1 confirmed the findings
332 obtained from confocal analysis. Additionally, VCE-004.8 exhibited a tendency to
333 increase the mRNA expression of Sirt1 in the non-ligated limb of CLI mice (Fig. 7C).
334
335 **Caveolin 1 is downregulated in CLI mice and human arteries.** To investigate the
336 effects of VCE-004.8 on the expression of other markers, we labeled the tissues with
337 αSMA to identify mature vessels. These vessels were subsequently isolated and studied
338 using Laser Capture Microdissection coupled to Mass Spectrometry (Fig. 8A). From the
339 total bulk of proteins (210), eleven proteins involved in the angiogenesis process were
340 identified according to Gene Ontology Annotations from Mice Genomic Identification [33].
341 Among them, caveolin 1 (CAV1) is of special interest in our study since its gene is
342 regulated by HIF-1[34] and it is required for collateral development in CLI mice [35] (Fig.
343 8B). The expression of CAV1 was detected in both the control limb of CLI mice and in
344 healthy human arteries (Fig. 8C and 8E), while it was downregulated in the ligated limb
345 of CLI mice and in arteries affected by PAD (Fig. 8C and 8E). Treatment with VCE-
346 004.8 normalized the expression of CAV1 protein and upregulated its mRNA expression
347 (Fig. 8C and 8D).
348
349 **DISCUSSION**
350
351 Effective induction and promotion of angiogenesis have been so far very challenging. A
352 better knowledge of the basic pro-angiogenic players will be crucial to achieve a clinical
353 benefit for PAD patients and other cardiovascular diseases. Therapeutic angiogenesis or
354 vascular regeneration remains an attractive treatment modality for PAD and chronic
355 tissue ischemia. Despite decades of research into angiogenic and cell-based therapies for
356 PAD, their translation to clinical use has been limited. Therefore, there is an urgent need
357 for novel therapeutic angiogenic approaches.
358 Vascular regeneration strategies include restoration of vascular function and
359 structure that can be partially achieved through HIF activation. While severe hypoxia can
360 be detrimental, leading to cell death and organ failure, mild hypoxia, also known as
361 hypoxia preconditioning, has shown promising therapeutic potential, particularly in the
362 treatment of cardiovascular diseases[36]. Mild hypoxia can be achieved by hypoxia mimetic

363 enzymatic inhibitors of PHDs such are JNJ-42041935, FG-4497, FG-4592 (Roxadustat),
364 TRC160334 (Desidustat), and AKB-4924 [37] or by novel PPA2/B55α activators such are
365 Etrinabdione (VCE-004.8) and VCE-005.1[13,38]. Indeed, it has been observed that the
366 enzymatic inhibitor of PHDs, FG-4497, confers protection against the development of
367 atherosclerosis, a pivotal factor in PAD pathogenesis [39]. Herein, we show the sprouting
368 and angiogenic activity of VCE-004.8 *in vitro* and *in vivo* and its efficacy in CLI mice
369 induced by femoral ligation. Etrinabdione induced endothelial cells proliferation,
370 angiogenic gene expression and prevented fibrosis. One striking and interesting
371 observation is that the effects of Etrinabdione occur only in the affected limbs compared
372 to non-ischemic limbs. A similar observation was found with sodium nitrite therapy and
373 metformin in CLI mice [40, 41] and these results agree with our previous finding showing
374 that VCE-004.8 induced angiogenesis and restored damaged brain blood barrier in the
375 affected brain hemisphere of mice with traumatic brain injury but in the contralateral
376 hemisphere [13]. Thus, we could speculate that the therapeutic benefit of Etrinabdione will
377 be akin to converting severe hypoxia into therapeutic mild hypoxia in the affected limb.
378 The pathophysiology of atherothrombosis and PAD is complex, and involves
379 many cells, proteins and pathways, giving the possibility to explore multitarget
380 therapeutic strategies, which by covering different angles of the disease may be beneficial
381 for the outcome of patients. Herein we show that Etrinabdione, a multitarget drug
382 candidate in clinical phases, induces HIF-1α expression in endothelial cells through a
383 novel pathway that potentially involves two axes: B55α/PHD2 and B55α/AMPK/Sirt1
384 signaling that may converge on HIF stabilization. In addition, VCE-004.8 induces the
385 phosphorylation of eNOS at ser1177, which is a target for AMPK. How B55α regulates
386 AMPK needs to be investigated at the molecular level but previous studies have revealed
387 that AMPK signaling regulates the nuclear accumulation of HIF-1α through a complex
388 process involving HDAC5 phosphorylation. This process leads to the export of HDAC5
389 from the nuclei to the cytosol, where it dissociates the complex formed by the HSP70
390 chaperone and nascent HIF-1α [42]. Subsequently, HIF-1α associates with HSP90,
391 facilitating its maturation and relocation into the nucleus. Notably, treatment with
392 CCT018159, an HSP90 inhibitor, partially inhibits VCE-004.8-induced HIF-1α
393 stabilization (Fig. S5). Moreover, Sirt1 interacts with AMPK and HIF-1α, and
394 pharmacological inhibition of Sirt1 impairs HIF-1α nuclear accumulation and the
395 expression of HIF-1α-dependent genes [43]. Therefore, it is probable that VCE-004.8

396 requires AMPK to enhance the synthesis of nascent HIF-1α, and B55α/PHD2 to stabilize
397 and translocate this nuclear factor into nuclei. This is supported by our results showing
398 that metformin, an AMPK activator that phosphorylates eNOS [39] but did not activate HIF-
399 1α in vascular endothelial cells[44]. However, it is noteworthy that metformin has been
400 shown to promote revascularization in CLI mice independently of HIF-1α [41].

401 In addition, VCE-004.8 is a dual agonist of PPARγ and CB_2R[14]. PPARγ and CB_2R
402 are preclinically validated therapeutic targets for vascular inflammation and
403 atherosclerosis [45,46,47]. For instance, foam cells play a vital role in the initiation and
404 development of atherosclerosis since they are the major sources of necrotic core in
405 atherosclerotic plaques. Interestingly, it has been shown that PPARγ agonists inhibit the
406 formation of macrophage foam cells *in vivo*[48]. Moreover, JHW-015, a CB_2R agonist,
407 significantly prevented oxLDL accumulation in foam cells and reduced the production of
408 proinflammatory cytokines and the expression of CD36, a scavenger receptor that plays
409 a critical role in the formation of foam cells. In agreement with finding CB_2R activation
410 by WIN55,212-2 also reduces an OxLDL-induced inflammatory response in rat
411 macrophages[49]. In line with this we have found that VCE-004.8 inhibits the induction of
412 foam cells in OxLDL-treated macrophages (Fig. S6).

413 On the other hand, VCE-004.8 has also shown efficacy in a murine model of
414 metabolic syndrome induced by high-fat diet. VCE-004.8 showed anti-obesity and anti-
415 inflammatory activity, prevented liver damage and significantly improved glycolipid
416 metabolism[17]. If this activity had translation in humans, we could expect an added benefit
417 in PAD patients with type II diabetes as co-morbidity. The same hold true for coexisting
418 cerebrovascular or coronary diseases since VCE-004.8 showed efficacy in a preclinical
419 stroke model with an excellent therapeutic window and inhibited angiotensin-II signaling
420 and cardiac inflammation and fibrosis[16,18].

421 In many cases, diseases with complex physiopathology are very difficult to be
422 treated by monotargeted therapies, and usually requires concomitant therapies
423 (polypharmacy) that have limitations such as therapy adherence and pharmacological
424 interactions. In contrast, multipronged therapies (polypharmacology) may represent
425 potential pharmacological therapies with better clinical benefits after providing a safe
426 profile in humans and an appropriated target engagement as it is the case of reprofiling
427 therapies with small molecules[50].

428

429 **CONCLUSIONS**

430 In conclusion, our results collectively demonstrate that VCE-004.8 is a first-in-class
431 activator of PP2A/B55α, a phosphatase critical for vascular endothelial cell homeostasis
432 through HIF-1 stabilization and activation. Furthermore, VCE-004.8 activates the
433 AMPK/Sirt1/eNOS pathway in a PP2A/B55α-dependent manner, showing potential in
434 preventing endothelial cell damage and senescence, while also promoting arteriogenesis
435 and angiogenesis in CLI mice. Moreover, the supplementary anti-inflammatory
436 properties of Etrinabdione position it as a potential disease-modifying drug, offering
437 clinical benefits to PAD patients with diverse comorbidities

438

439 **ACKNOWLEDGMENTS**

440 We acknowledge the Microscopy Advanced Optical Microscopy and the Proteomic Units
441 of IMIBIC for its support.

442

443 **SOURCES OF FUNDING**

444 This work was supported by grants PID2020-114753RB-I00 (Agencia Estatal de
445 Investigación, Spain; co-funded with EU funds from FEDER Program) and CPP2021-
446 008557/AEI/10.13039/501100011033/Unión Europea NextGenerationEU/PRTR.

447

448 **DISCLOSURES**

449 AGM, ILC, and EM have applied for a European Patent based on some of the data
450 presented herein.

REFERENCES

1. Annex BH, Cooke JP. New Directions in Therapeutic Angiogenesis and Arteriogenesis in Peripheral Arterial Disease. *Circ Res*. 2021;128:1944–1957.
2. Beckman JA, Schneider PA, Conte MS. Advances in Revascularization for Peripheral Artery Disease: Revascularization in PAD. *Circ Res*. 2021;128:1885–1912.
3. Clark AR, Ohlmeyer M. Protein phosphatase 2A as a therapeutic target in inflammation and neurodegeneration. *Pharmacology & Therapeutics*. 2019;201:181–201.
4. Di Conza G, Trusso Cafarello S, Loroch S, Mennerich D, Deschoemaeker S, Di Matteo M, Ehling M, Gevaert K, Prenen H, Zahedi RP, et al. The mTOR and PP2A Pathways Regulate PHD2 Phosphorylation to Fine-Tune HIF1α Levels and Colorectal Cancer Cell Survival under Hypoxia. *Cell Reports*. 2017;18:1699–1712.
5. Appelhoff RJ, Tian Y-M, Raval RR, Turley H, Harris AL, Pugh CW, Ratcliffe PJ, Gleadle JM. Differential Function of the Prolyl Hydroxylases PHD1, PHD2, and PHD3 in the Regulation of Hypoxia-inducible Factor. *Journal of Biological Chemistry*. 2004;279:38458–38465.
6. Watts ER, Walmsley SR. Inflammation and Hypoxia: HIF and PHD Isoform Selectivity. *Trends in Molecular Medicine*. 2019;25:33–46.
7. Olenchock BA, Moslehi J, Baik AH, Davidson SM, Williams J, Gibson WJ, Chakraborty AA, Pierce KA, Miller CM, Hanse EA, et al. EGLN1 Inhibition and Rerouting of α-Ketoglutarate Suffice for Remote Ischemic Protection. *Cell*. 2016;164:884–895.
8. Liang Y, Ruan W, Jiang Y, Smalling R, Yuan X, Eltzschig HK. Interplay of hypoxia-inducible factors and oxygen therapy in cardiovascular medicine. *Nat Rev Cardiol*. 2023;20:723–737.
9. Ehling M, Celus W, Martín-Pérez R, Alba-Rovira R, Willox S, Ponti D, Cid MC, Jones EAV, Di Conza G, Mazzone M. B55α/PP2A Limits Endothelial Cell Apoptosis During Vascular Remodeling: A Complementary Approach To Disrupt Pathological Vessels? *Circ Res*. 2020;127:707–723.
10. Ministrini S, Puspitasari YM, Beer G, Liberale L, Montecucco F, Camici GG. Sirtuin 1 in Endothelial Dysfunction and Cardiovascular Aging. *Front. Physiol.* 2021;12:733696.
11. Han Y, Kim SY. Endothelial senescence in vascular diseases: current understanding and future opportunities in senotherapeutics. *Exp Mol Med*. 2023;55:1–12.
12. D'Onofrio N, Vitiello M, Casale R, Servillo L, Giovane A, Balestrieri ML. Sirtuins in vascular diseases: Emerging roles and therapeutic potential. *Biochimica et Biophysica Acta (BBA) - Molecular Basis of Disease*. 2015;1852:1311–1322.
13. Navarrete C, Carrillo-Salinas F, Palomares B, Mecha M, Jiménez-Jiménez C, Mestre L, Feliú A, Bellido ML, Fiebich BL, Appendino G, et al. Hypoxia mimetic activity of VCE-004.8, a cannabidiol quinone derivative: implications for multiple sclerosis therapy. *J Neuroinflammation*. 2018;15:64
14. Del Río C, Navarrete C, Collado JA, Bellido ML, Gómez-Cañas M, Pazos MR, Fernández-Ruiz J, Pollastro F, Appendino G, Calzado MA, et al. The cannabinoid quinol VCE-004.8 alleviates bleomycin-induced scleroderma and exerts potent antifibrotic effects through peroxisome proliferator-activated receptor-γ and CB2 pathways. *Sci Rep*. 2016;6:21703.
15. Navarrete C, García-Martín A, Correa-Sáez A, Prados ME, Fernández F, Pineda R,

Mazzone M, Álvarez-Benito M, Calzado MA, Muñoz E. A cannabidiol aminoquinone derivative activates the PP2A/B55α/HIF pathway and shows protective effects in a murine model of traumatic brain injury. *J Neuroinflammation*. 2022;19:177.

16. García-Martín A, Navarrete C, Garrido-Rodríguez M, Prados ME, Caprioglio D, Appendino G, Muñoz E. EHP-101 alleviates angiotensin II-induced fibrosis and inflammation in mice. *Biomedicine & Pharmacotherapy*. 2021;142:112007.
17. Palomares B, Ruiz-Pino F, Navarrete C, Velasco I, Sánchez-Garrido MA, Jimenez-Jimenez C, Pavicic C, Vazquez MJ, Appendino G, Bellido ML, et al. VCE-004.8, A Multitarget Cannabinoquinone, Attenuates Adipogenesis and Prevents Diet-Induced Obesity. *Sci Rep*. 2018;8:16092.
18. Lavayen BP, Yang C, Larochelle J, Liu L, Tishko RJ, De Oliveira ACP, Muñoz E, Candelario-Jalil E. Neuroprotection by the cannabidiol aminoquinone VCE-004.8 in experimental ischemic stroke in mice. *Neurochemistry International*. 2023;165:105508.
19. Claesson-Welsh L, Dejana E, McDonald DM. Permeability of the Endothelial Barrier: Identifying and Reconciling Controversies. *Trends in Molecular Medicine*. 2021;27:314–331.
20. Rodríguez C, Muñoz M, Contreras C, Prieto D. AMPK, metabolism, and vascular function. *The FEBS Journal*. 2021;288:3746–3771.
21. Dengler F. Activation of AMPK under Hypoxia: Many Roads Leading to Rome. *IJMS*. 2020;21:2428.
22. Cantó C, Gerhart-Hines Z, Feige JN, Lagouge M, Noriega L, Milne JC, Elliott PJ, Puigserver P, Auwerx J. AMPK regulates energy expenditure by modulating NAD+ metabolism and SIRT1 activity. *Nature*. 2009;458:1056–1060.
23. Lan F, Cacicedo JM, Ruderman N, Ido Y. SIRT1 Modulation of the Acetylation Status, Cytosolic Localization, and Activity of LKB1. *Journal of Biological Chemistry*. 2008;283:27628–27635.
24. Cooke JP, Meng S. Vascular Regeneration in Peripheral Artery Disease. *ATVB*. 2020;40:1627–1634.
25. Wahlberg E. Angiogenesis and arteriogenesis in limb ischemia. *Journal of Vascular Surgery*. 2003;38:198–203.
26. Han J, Luo L, Marcelina O, Kasim V, Wu S. Therapeutic angiogenesis-based strategy for peripheral artery disease. *Theranostics*. 2022;12:5015–5033.
27. Yang J, Ii M, Kamei N, Alev C, Kwon S-M, Kawamoto A, Akimaru H, Masuda H, Sawa Y, Asahara T. CD34+ Cells Represent Highly Functional Endothelial Progenitor Cells in Murine Bone Marrow. *PLoS ONE*. 2011;6:e20219.
28. Van Huyen J-PD, Smadja DM, Bruneval P, Gaussem P, Dal-Cortivo L, Julia P, Fiessinger J-N, Cavazzana-Calvo M, Aiach M, Emmerich J. Bone marrow-derived mononuclear cell therapy induces distal angiogenesis after local injection in critical leg ischemia. *Modern Pathology*. 2008;21:837–846.
29. Dong Z, Pan T, Fang Y, Wei Z, Gu S, Fang G, Liu Y, Luo Y, Liu H, Zhang T, et al. Purified CD34+ cells versus peripheral blood mononuclear cells in the treatment of angiitis-induced no-option critical limb ischaemia: 12-Month results of a prospective randomised single-blinded non-inferiority trial. *EBioMedicine*. 2018;35:46–57.
30. Calvier L, Miana M, Reboul P, Cachofeiro V, Martinez-Martinez E, De Boer RA, Poirier F, Lacolley P, Zannad F, Rossignol P, et al. Galectin-3 Mediates Aldosterone-Induced Vascular Fibrosis. *ATVB*. 2013;33:67–75.
31. Ding N, Yang C, Ballew SH, Kalbaugh CA, McEvoy JW, Salameh M, Aguilar D, Hoogeveen RC, Nambi V, Selvin E, et al. Fibrosis and Inflammatory Markers and

Long-Term Risk of Peripheral Artery Disease: The ARIC Study. *ATVB*. 2020;40:2322–2331.

32. Bhattacharyya S, Wang W, Morales-Nebreda L, Feng G, Wu M, Zhou X, Lafyatis R, Lee J, Hinchcliff M, Feghali-Bostwick C, et al. Tenascin-C drives persistence of organ fibrosis. *Nat Commun*. 2016;7:11703.
33. Eppig JT. Mouse Genome Informatics (MGI) Resource: Genetic, Genomic, and Biological Knowledgebase for the Laboratory Mouse. *ILAR Journal*. 2017;58:17–41.
34. Wang Y, Roche O, Xu C, Moriyama EH, Heir P, Chung J, Roos FC, Chen Y, Finak G, Milosevic M, et al. Hypoxia promotes ligand-independent EGF receptor signaling via hypoxia-inducible factor–mediated upregulation of caveolin-1. *Proc. Natl. Acad. Sci. U.S.A.* 2012;109:4892–4897.
35. Sonveaux P, Martinive P, DeWever J, Batova Z, Daneau G, Pelat M, Ghisdal P, Grégoire V, Dessy C, Balligand J-L, et al. Caveolin-1 Expression Is Critical for Vascular Endothelial Growth Factor–Induced Ischemic Hindlimb Collateralization and Nitric Oxide–Mediated Angiogenesis. *Circulation Research*. 2004;95:154–161.
36. Bagali S, Das KK. Hypoxia and its preconditioning on cardiac and vascular remodelling in experimental animals. *Respiratory Physiology & Neurobiology*. 2021;285:103588.
37. Joharapurkar AA, Pandya VB, Patel VJ, Desai RC, Jain MR. Prolyl Hydroxylase Inhibitors: A Breakthrough in the Therapy of Anemia Associated with Chronic Diseases. *J. Med. Chem.* 2018;61:6964–6982.
38. Prados ME, Correa-Sáez A, Unciti-Broceta JD, Garrido-Rodríguez M, Jimenez-Jimenez C, Mazzone M, Minassi A, Appendino G, Calzado MA, Muñoz E. Betulinic Acid Hydroxamate is Neuroprotective and Induces Protein Phosphatase 2A-Dependent HIF-1α Stabilization and Post-transcriptional Dephosphorylation of Prolyl Hydrolase 2. *Neurotherapeutics*. 2021;18:1849–1861.
39. Rahtu-Korpela L, Määttä J, Dimova EY, Hörkkö S, Gylling H, Walkinshaw G, Hakkola J, Kivirikko KI, Myllyharju J, Serpi R, et al. Hypoxia-Inducible Factor Prolyl 4-Hydroxylase-2 Inhibition Protects Against Development of Atherosclerosis. *ATVB*. 2016;36:608–617.
40. Kumar D, Branch BG, Pattillo CB, Hood J, Thoma S, Simpson S, Illum S, Arora N, Chidlow JH, Langston W, et al. Chronic sodium nitrite therapy augments ischemia-induced angiogenesis and arteriogenesis. *Proc. Natl. Acad. Sci. U.S.A.* 2008;105:7540–7545.
41. Takahashi N, Shibata R, Ouchi N, Sugimoto M, Murohara T, Komori K. Metformin stimulates ischemia-induced revascularization through an eNOS dependent pathway in the ischemic hindlimb mice model. *Journal of Vascular Surgery*. 2015;61:489–496.
42. Chen S, Yin C, Lao T, Liang D, He D, Wang C, Sang N. AMPK-HDAC5 pathway facilitates nuclear accumulation of HIF-1α and functional activation of HIF-1 by deacetylating Hsp70 in the cytosol. *Cell Cycle*. 2015;14:2520–2536.
43. Laemmle A, Lechleiter A, Roh V, Schwarz C, Portmann S, Furer C, Keogh A, Tschan MP, Candinas D, Vorburger SA, et al. Inhibition of SIRT1 Impairs the Accumulation and Transcriptional Activity of HIF-1α Protein under Hypoxic Conditions. *PLoS ONE*. 2012;7:e33433.
44. Prados ME, Navarrete C, García-Martín A, Lastres-Cubillo I, Ponce-Díaz F, Martínez-Orgado J, Muñoz E. VCE-005.1, an hypoxia mimetic betulinic acid derivative, induces angiogenesis and shows efficacy in a murine model of traumatic brain injury. *Biomedicine & Pharmacotherapy*. 2023;162:114715.

45. Yang X, Shang D. The role of peroxisome proliferator-activated receptor γ in lipid metabolism and inflammation in atherosclerosis. *Cell Biology International*. 2023;47:1469–1487.
46. Xu X, Guo H, Jing Z, Yang L, Chen C, Peng L, Wang X, Yan L, Ye R, Jin X, et al. N-Oleoylethanolamine Reduces Inflammatory Cytokines and Adhesion Molecules in TNF-α-induced Human Umbilical Vein Endothelial Cells by Activating CB2 and PPAR-α. *Journal of Cardiovascular Pharmacology*. 2016;68:280–291.
47. Steffens S, Pacher P. Targeting cannabinoid receptor CB_2 in cardiovascular disorders: promises and controversies. *British J Pharmacology*. 2012;167:313–323.
48. Li AC, Binder CJ, Gutierrez A, Brown KK, Plotkin CR, Pattison JW, Valledor AF, Davis RA, Willson TM, Witztum JL, et al. Differential inhibition of macrophage foam-cell formation and atherosclerosis in mice by PPARα, β/δ, and γ. *J. Clin. Invest.* 2004;114:1564–1576.
49. Turcotte C, Blanchet M-R, Laviolette M, Flamand N. The CB2 receptor and its role as a regulator of inflammation. *Cell. Mol. Life Sci.* 2016;73:4449–4470.
50. Ryszkiewicz P, Malinowska B, Schlicker E. Polypharmacology: promises and new drugs in 2022. *Pharmacol. Rep*. 2023;75:755–770.

620 **FIGURE LEGENDS**

621

622 **Figure 1**. **VCE-004.8 induces B55α/PP2A expression and activates HIF-1α in**
623 **endothelial EA.hy926 cells. A,** Representative images of B55α expression in EA.hy926
624 cells untreated and treated with VCE-004.8 for 24 h. Magnified region (marked by the
625 white rectangle) shows preferential perinuclear expression of B55α as indicated by white
626 arrows. **B,** EA.hy926 cells were transfected with siB55α or scrambled siRNAs (siCTR)
627 and 48 h later treated with VCE-004.8 for 3 h. B55α and HIF-1α protein expression was
628 analyzed by immunoblotting. **C,** Effect of VCE-004.8 on cell viability. EA.hy926 cells
629 were pre-incubated with increasing concentrations of VCE-004.8 during 1 h and then
630 were exposed to H_2O_2 for 24 h. Cell viability was calculated by MTT assay. The data
631 passed the normality test performed by the Kolmogorov-Smirnov test. P value is
632 calculated using 1-way ANOVA followed by Tukey post hoc multiple comparisons to
633 compare between the groups (n>4 independent experiments per group), the results are
634 shown as mean ± SEM. **D**, The cytoprotection mediated by VCE-004.8 is partially
635 dependent on HIF-1α activation. EA.hy926 cells were pretreated with VCE-004.8 in the
636 absence and the presence of the HIF-1α inhibitor YC-1 and then exposed to H_2O_2. Cell
637 viability was calculated by MTT assay. The data passed the normality test performed by
638 the Shaphiro-Wilk test. P value is calculated using 1-way ANOVA followed by Tukey
639 post hoc multiple comparisons to compare between the groups (n>3 independent
640 experiments per group); the results are shown as means ± SEM. P values indicated in
641 panels, significant as **p<0.01, ***p<0.001 ****p<0.0001.

642

643 **Figure 2**. **VCE-004.8 activates AMPK/Sirt1 pathway and prevents cellular**
644 **senescence**. **A,** HEK-293T cells preincubated with or without DS for 30 min and
645 stimulated for 3 h with increasing concentrations of VCE-004.8 and the steady state levels
646 of pAMPK total AMPK and actin detected by western blot. **B,** EA.hy296 cells were
647 stimulated with VCE-004.8 for 3h and the expression of Sirt1 and Visfatin (NAMPT) was
648 analyzed by western blot. **C,** VCE-004.8 induces Sirt1 activity measured by a
649 fluorometric assay. SRT1720 was used as a positive control. Data represent the mean ±
650 SD (n = 3). **D,** NAD^+/NADH ratio was determined in EA.hy296 cells with a NAD^+
651 /NADH assay kit. The data passed the normality test performed by the Shaphiro-Wilk
652 test. P value is calculated using 1-way ANOVA followed by Tukey post hoc multiple

653 comparisons to compare between the groups (n=3 independent experiments per group);
654 the results are shown as means ± SEM. P value indicated in panel, significant as **p<0.01.
655 **E,** VCE-004.8 prevents H_2O_2-induced senescence measured by SA-β-gal staining in
656 HMEC-1 cells. The data passed the normality test performed by the D'Agostino &
657 Pearson test. P value is calculated using 1-way ANOVA followed by Tukey post hoc
658 multiple comparisons to compare between the groups (n>18 represent areas of cell surface
659 from 3 independent experiments), the results are shown as means ± SD. P values indicated
660 in panel, significant as ****p<0.0001. **F,** HMEC-1 cells were incubated with VCE-004.8
661 and exposed to H_2O_2 and the expression of Sirt1, p21 and tubulin detected by western
662 blot.
663
664 **Figure 3**. **VCE-004.8 induces eNOS activation and NO synthesis in a B55α**
665 **dependent manner.** **A**. EA.hy926 cells were treated with VCE-004.8 for 3 h
666 Representative western blot of three independent experiments is shown. **B,** VCE-004.8
667 induces NO production. EA.hy296 cells were seeded, preincubated with DAF-2DA and
668 treated with sulforaphane (50 μM) or VCE-004.8 (10μM). The figure indicated the
669 percentage NO induction. The data passed the normality test performed by the Shaphiro-
670 Wilk test. P value is calculated using 1-way ANOVA followed by Tukey post hoc
671 multiple comparisons to compare between the groups (n=3 independent experiments per
672 group); the results are shown as means ± SD. P value indicated in panel, significant as
673 ****p<0.0001. **C,** VCE-004.8 induces eNOS phosphorylation in vascular endothelial
674 cells in a B55α dependent manner. EA.hy296 cells were transfected with siB55α or
675 scrambled siRNAs (siCTR) and 48 h later treated with VCE-004.8 for 3 h. Representative
676 western blot of three independent experiments is shown.
677
678 **Figure 4**. **Effects of oral VCE-004.8 in a Critical Limb Ischemia mouse model**. **A,**
679 Representative whole-mount images of Microfil vascular cast limbs 10 days after
680 ischemia, Micro-CT reconstruction and their segmentation of arterial vasculature 28 days
681 after femoral artery ligation. Collateral artery growth is indicated by black arrows. **B,**
682 Expression of *Vegf-a*, *Epo*, *Hgf*, and *Hif1α* mRNA in the gastrocnemius after 10 days of
683 ischemia. The data passed the normality test performed by the Shaphiro-Wilk test. P value
684 is calculated using 1-way ANOVA followed by Tukey post hoc multiple comparisons to

685 compare between the groups (n=3 animals per group); the results are shown as means ±
686 SEM. P value indicated in panel, significant as *p < 0.05; **p < 0.01.
687
688 **Figure 5**. **Oral VCE-004.8 enhances ischemia-induced vessel formation and vascular**
689 **endothelial cells proliferation *in vivo*. A.** Double immunofluorescence confocal staining
690 of α-SMA (green)/CD31 (red) in gastrocnemius muscles 28 day after ischemia. The
691 immunofluorescence was used to quantify the number of vessel peer area and the
692 perimeter of the lumen vessel in mouse muscle. As the data cannot passed the normality
693 test. P values are calculated using a nonparametric Kruskal-Wallis test followed by Dunn
694 multiple. The results are shown as mean ± SEM. P values indicated in panels, significant
695 as **p < 0.01, ***p<0.001, ****p<0.0001. **B,** The number of $CD31^+/Ki67^+$ positive cells
696 per area and number of $CD31^+/Ki67^+$ cells per total cells were quantified using double
697 immunofluorescence confocal staining of CD31 (green) and Ki67 (red) in gastrocnemius
698 muscles 28 day after ischemia. Significance was determined by one-way ANOVA
699 followed by Tukey´s test. The results are shown as means ± SEM (n=3). P values
700 indicated in panels, significant as ****p < 0.0001.
701
702 **Figure 6**. **Oral VCE-004.8 enhanced ischemia-induced *de novo* vessel and alleviated**
703 **fibrosis *in vivo*. A,** Double immunofluorescence confocal staining of CD34
704 (green)/CD31 (red) in gastrocnemius muscles 28 days was used to calculate the number
705 of $CD34^+/CD31^-$ cells (immature endothelial vascular cells) and $CD34^+/CD31^+$ (mature
706 endothelial vascular cells). Values are mean ± SEM (n = 3-4). In both quantifications, the
707 significance was determined by one-way ANOVA non-parametric followed by a
708 Kruskal–Wallis test. P values indicated in panels, significant as **p < 0,01; ***p < 0.001;
709 ****p < 0.0001. **B,** Immunofluorescence staining of TNC (green) in gastrocnemius
710 muscles 28 days after ischemia and quantifications. Values are mean ± SEM (n = 3-4),
711 and significance was determined by one-way ANOVA non-parametric followed by
712 Kruskal–Wallis test. P values indicated in panels, significant as ***p < 0.001; ****p <
713 0.0001. **C,** Representative immunofluorescence staining of TNC in cross-section of
714 healthy and disease human arteries.
715
716 **Figure 7**. **Effects of VCE-004.8 on B55α and Sirt1 expression *in vivo*. A,**
717 Representative double immunofluorescence confocal staining of B55α (red)/CD31
718 (green) (left) and immunofluorescence staining of Sirt1(green) (right) in gastrocnemius

719 muscles 10 days after ischemia. **B,** Quantifications of B55α (left) and Sirt1 (right)
720 staining in gastrocnemius muscles 10 days after ischemia. For B55α and Sirt1
721 quantification, the data do not pass the normality test performed and the significance was
722 determined non-parametric followed by a Kruskal–Wallis test. Values are mean ± SEM
723 (n = 3-4). P values indicated in panels, significant as *p < 0.05 as **p < 0.01; ***p <
724 0.001. **C,** Expression of *B55α* and *Sirt1* mRNA in mice gastrocnemius at 10 days after
725 femoral ligation. The data passed the normality test performed by the Shaphiro-Wilk test.
726 P value is calculated using 1-way ANOVA followed by Tukey post hoc multiple
727 comparisons to compare between the groups (n=3 animals per group). The results are
728 shown as mean ± SEM. P value indicated in panel, significant as *p < 0.05; **p < 0.01;
729 ***p < 0.001; ****p < 0.0001. **D,** Representative immunofluorescence image of
730 B55α (red) in cross-section of healthy and disease human arteries (left) and representative
731 double immunofluorescence staining of Sirt1 (green) and CD31(red) in cross-section of
732 healthy and disease human arteries (right). Magnified region (white rectangle) showing
733 details of Sirt1 expression (yellow arrow).
734
735 **Figure 8**. **Oral VCE-004.8 induces CAV1 *in vivo*.** **A**, Overview of laser capture
736 microdissection. Representative images vessel marked with αSMA in gastrocnemius
737 before (left) and after (right) laser dissection indicated by red asterisk. **B**, Heatmap
738 showing the expression levels for the resulting list of 11 proteins. Color indicates the
739 mean of scaled regularized log transformed expression values. Red square indicates
740 CAV1. **C.** Representatives images of double immunostaining of CAV1(red) and CD31
741 (green) in gastrocnemius 10 days after ischemia (left) and the CAV1 staining
742 quantification (right). The significance was determined non-parametric followed by a
743 Kruskal–Wallis test. In both quantification, values are mean ± SEM, (n = 3). P values
744 indicated in panels, significant as *p < 0.05. **D,** The expression of *Cav1* mRNA in mice
745 gastrocnemius at 10 days. The data passed the normality test performed by the Shaphiro-
746 Wilk test. P value is calculated using 1-way ANOVA followed by Tukey post hoc
747 multiple comparisons to compare between the groups test (n=3 animals per group). The
748 results are shown as mean ± SEM. Values indicated in panels, significant as *p < 0.05;
749 **p < 0.01. **E,** Representative immunofluorescence staining of CAV1 in cross-section of
750 healthy and disease human arteries.
751

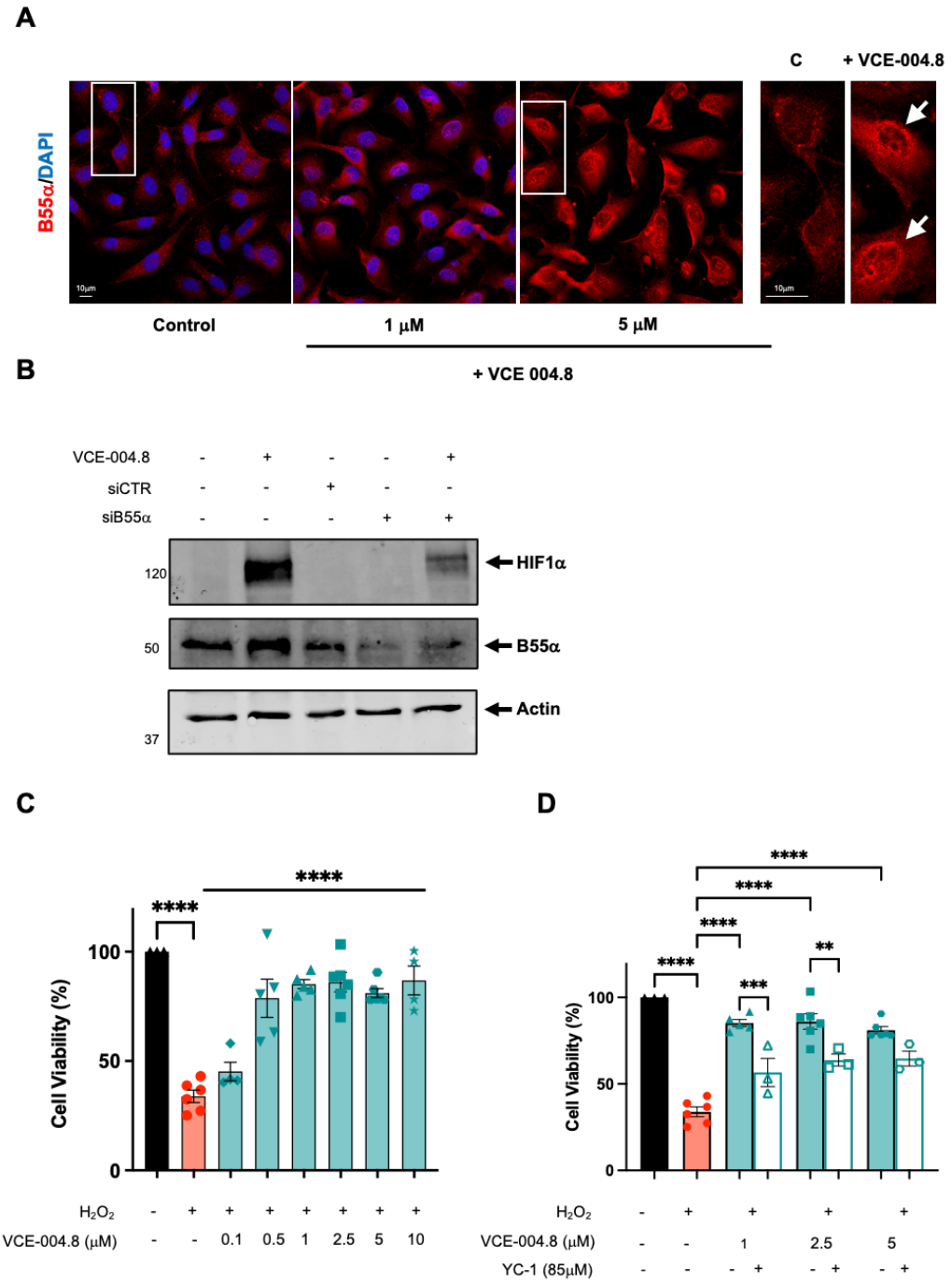
A
C
+ VCE-004.8
B55α/DAPI
Control
1 µM
5 µM
+ VCE 004.8
B
VCE-004.8
siCTR
siB55α
HIF1α
B55α
Actin
120
50
37
C
D
Cell Viability (%)
H2O2
VCE-004.8 (µM)
YC-1 (85µM)

Figure 1

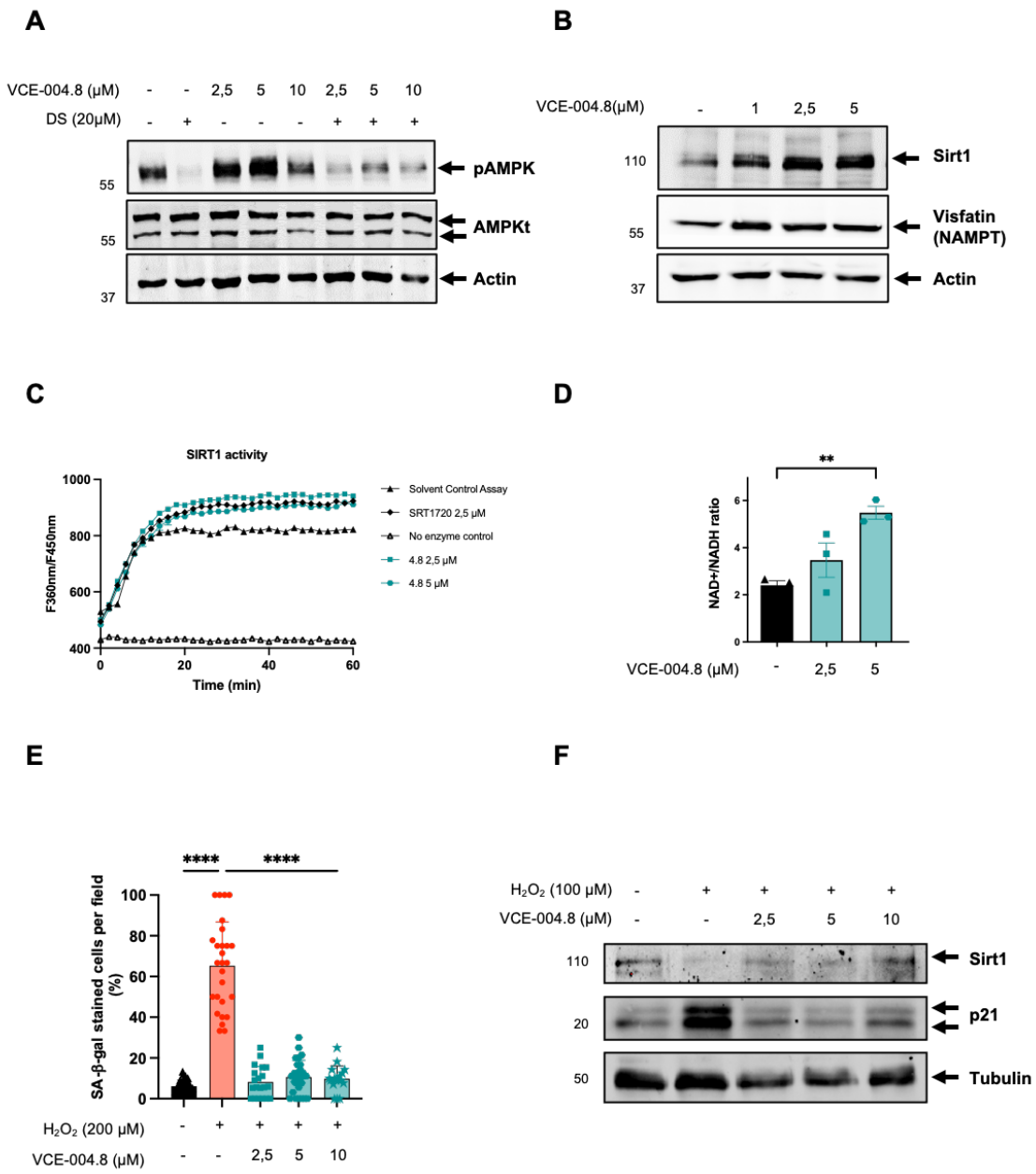
A
VCE-004.8 (μM) - - 2,5 5 10 2,5 5 10
DS (20μM) - + - - - + + +
55
55
37
pAMPK
AMPKt
Actin
B
VCE-004.8(μM) - 1 2,5 5
110
55
37
Sirt1
Visfatin (NAMPT)
Actin
C
SIRT1 activity
F360nm/F450nm
1000
800
600
400
0
20
40
60
Time (min)
Solvent Control Assay
SRT1720 2,5 μM
No enzyme control
4.8 2,5 μM
4.8 5 μM
D
**
NAD+/NADH ratio
6
4
2
0
VCE-004.8 (μM) - 2,5 5
E
****
****
SA-β-gal stained cells per field (%)
100
80
60
40
20
0
H2O2 (200 μM) - + + + +
VCE-004.8 (μM) - - 2,5 5 10
F
H2O2 (100 μM) - + + + +
VCE-004.8 (μM) - - 2,5 5 10
110
20
50
Sirt1
p21
Tubulin

Figure 2

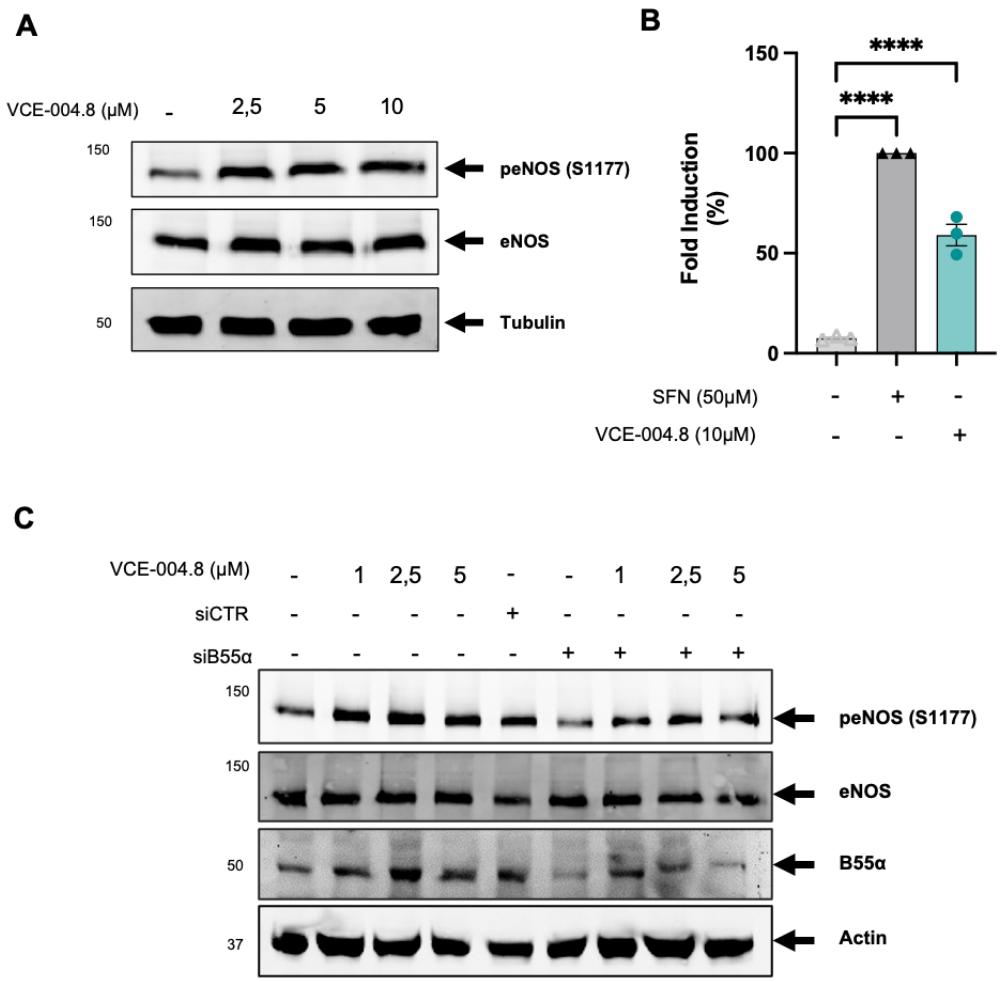
A
VCE-004.8 (μM)
-
2,5
5
10
150
150
50
peNOS (S1177)
eNOS
Tubulin
B
150
100
50
0
Fold Induction (%)
****
****
SFN (50μM)
VCE-004.8 (10μM)
C
VCE-004.8 (μM)
siCTR
siB55α
150
150
50
37
peNOS (S1177)
eNOS
B55α
Actin

Figure 3

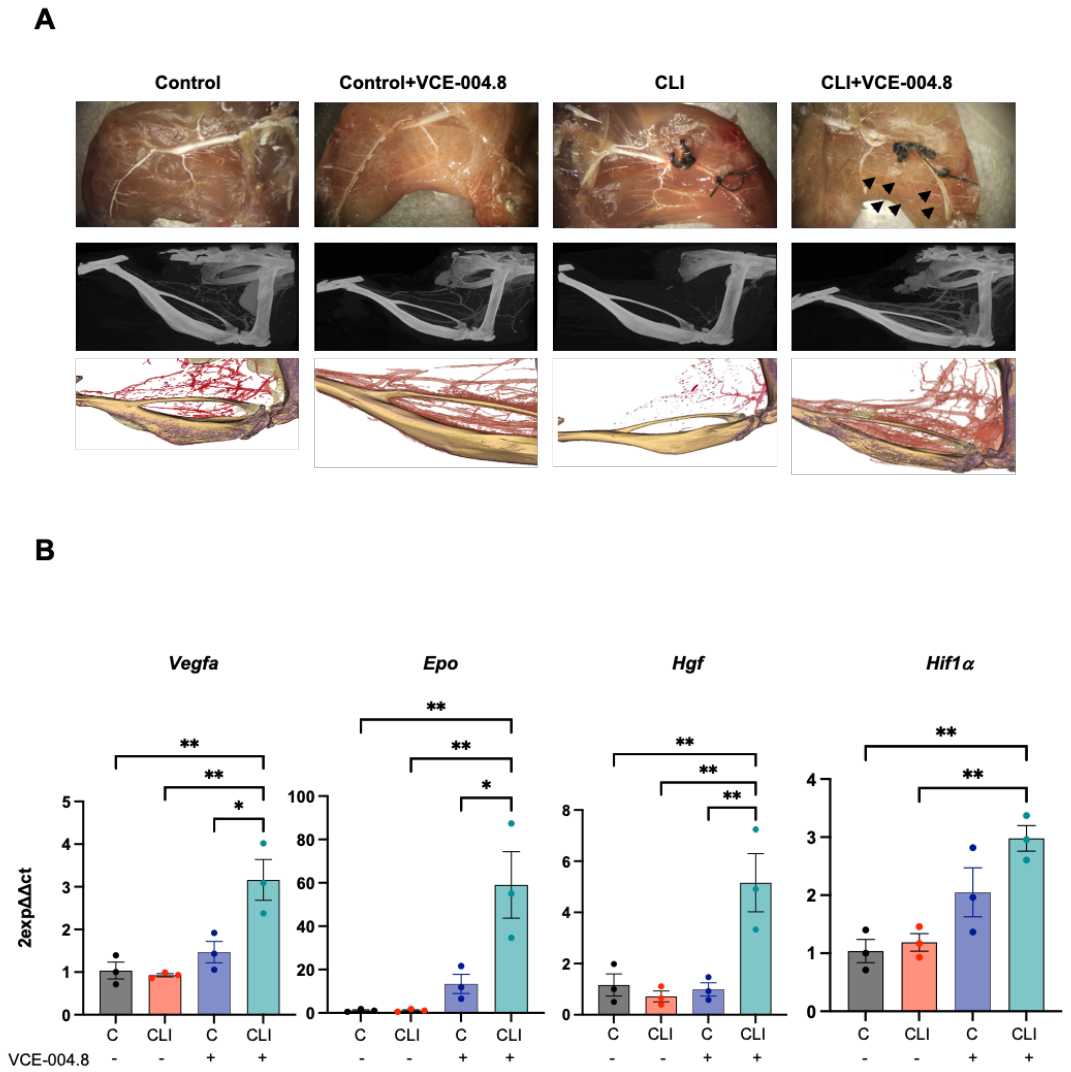
A
Control
Control+VCE-004.8
CLI
CLI+VCE-004.8
B
Vegfa
Epo
Hgf
Hif1α
2expΔΔct
C
CLI
C
CLI
VCE-004.8
-
-
+
+
**
*

Figure 4

783

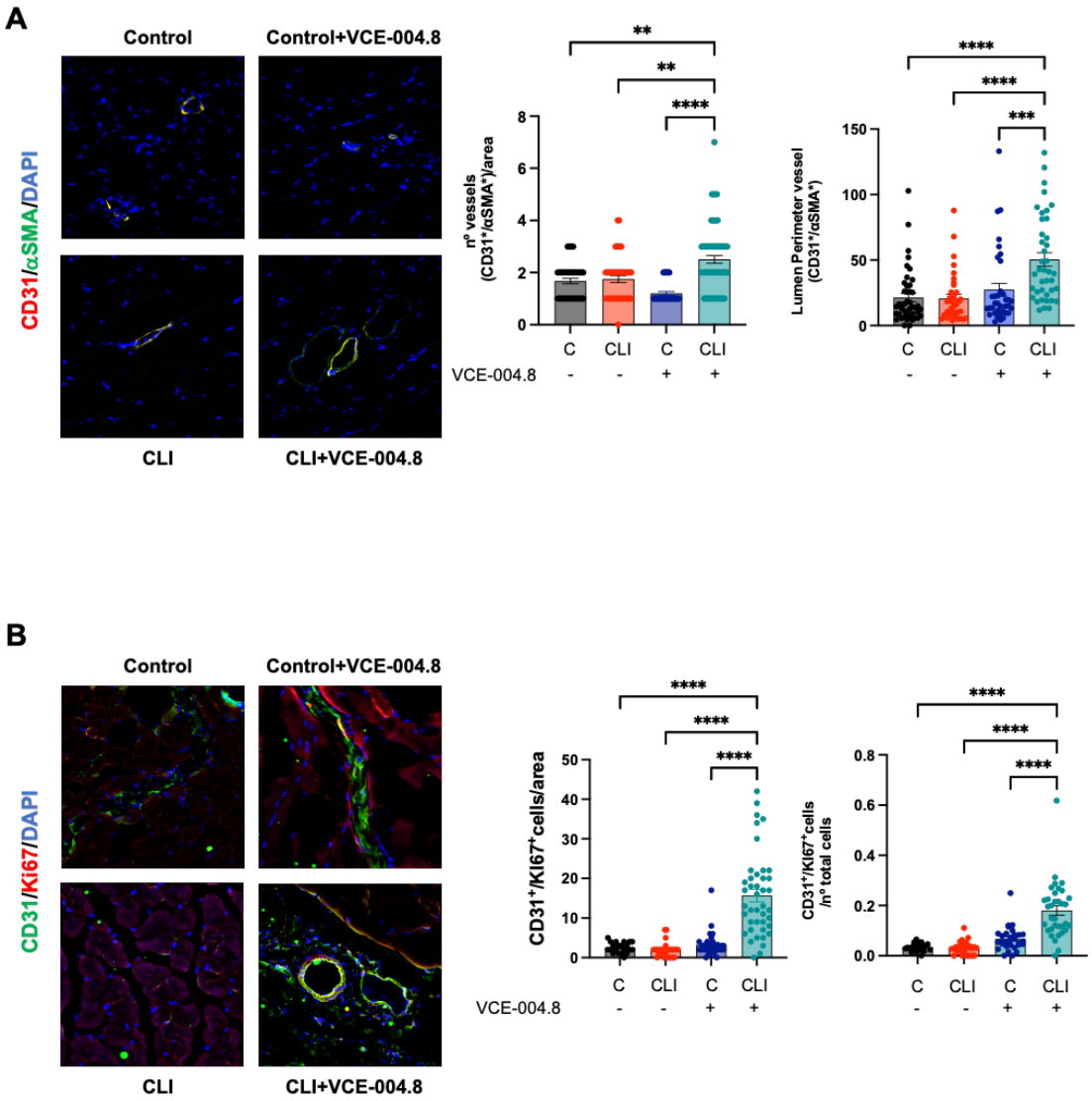

Figure 5

784

785

786

787

788

789

790

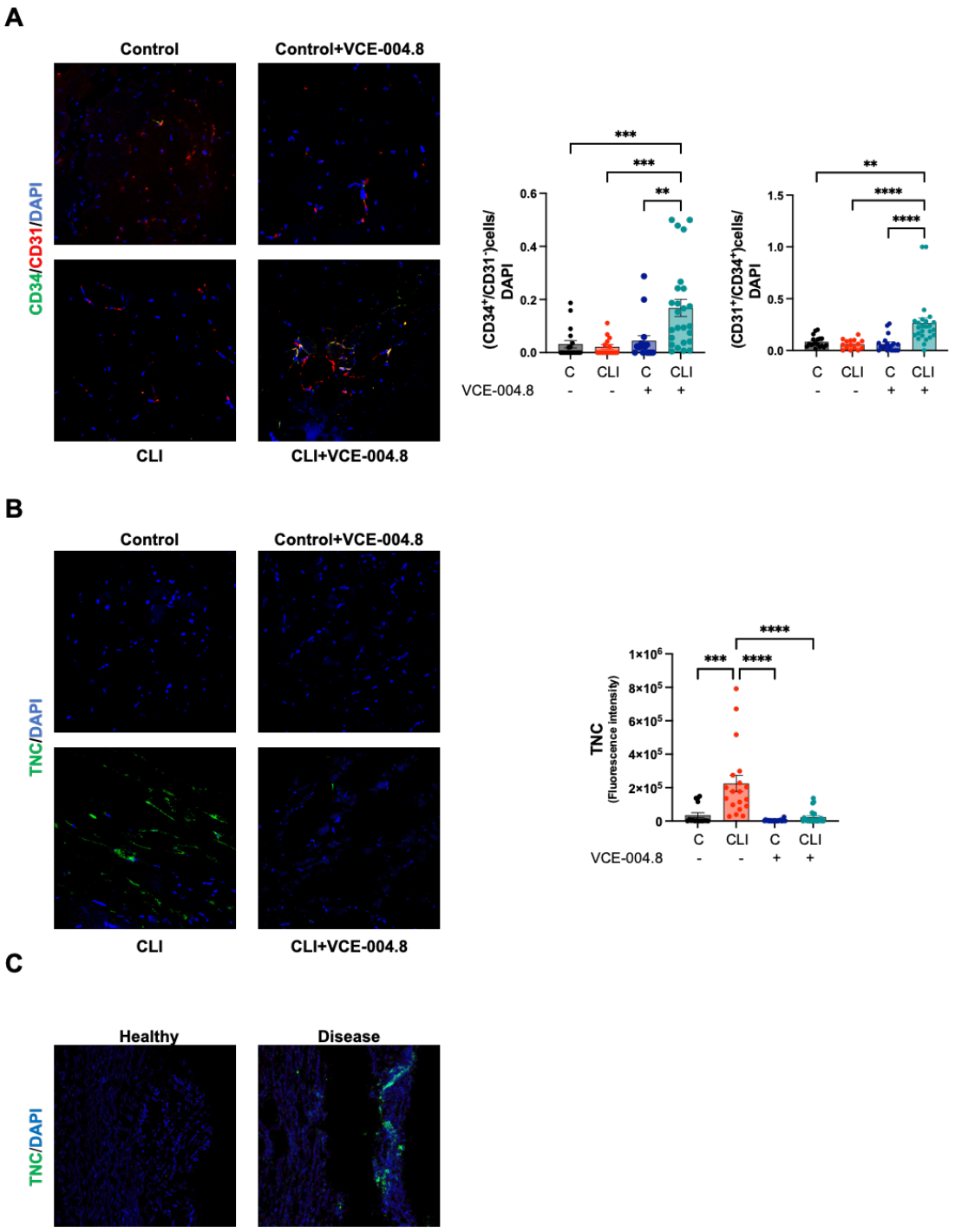
A
Control
Control+VCE-004.8
CD34/CD31/DAPI
CLI
CLI+VCE-004.8
(CD34+/CD31-)cells/ DAPI
(CD31+/CD34+)cells/ DAPI
C
CLI
VCE-004.8
B
TNC/DAPI
TNC (Fluorescence intensity)
C
Healthy
Disease

Figure 6

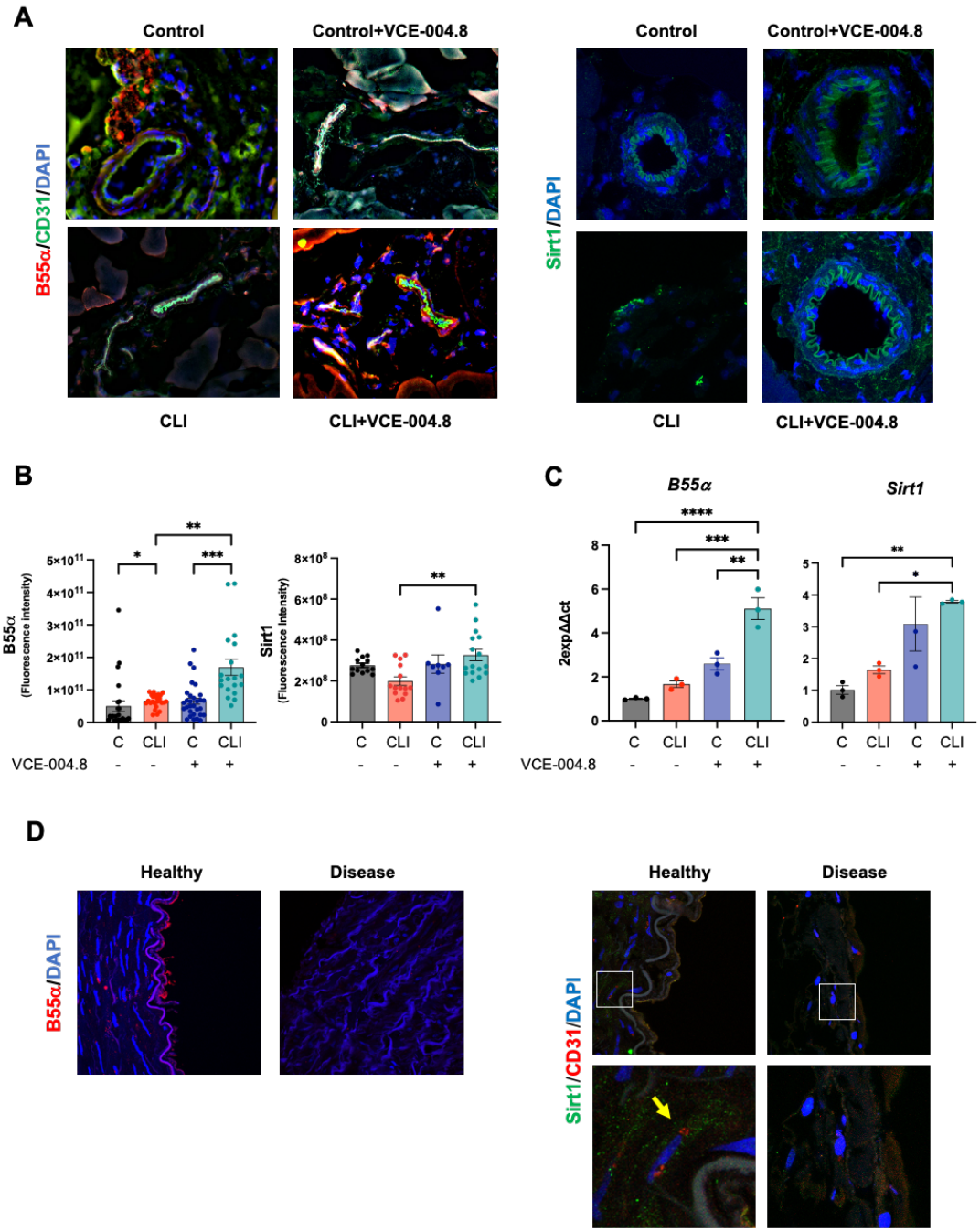
A
Control
Control+VCE-004.8
B55α/CD31/DAPI
CLI
CLI+VCE-004.8
Control
Control+VCE-004.8
Sirt1/DAPI
CLI
CLI+VCE-004.8
B
B55α
(Fluorescence intensity)
Sirt1
(Fluorescence Intensity)
C
C
CLI
VCE-004.8
B55α
Sirt1
2expΔΔct
D
Healthy
Disease
B55α/DAPI
Healthy
Disease
Sirt1/CD31/DAPI

Figure 7

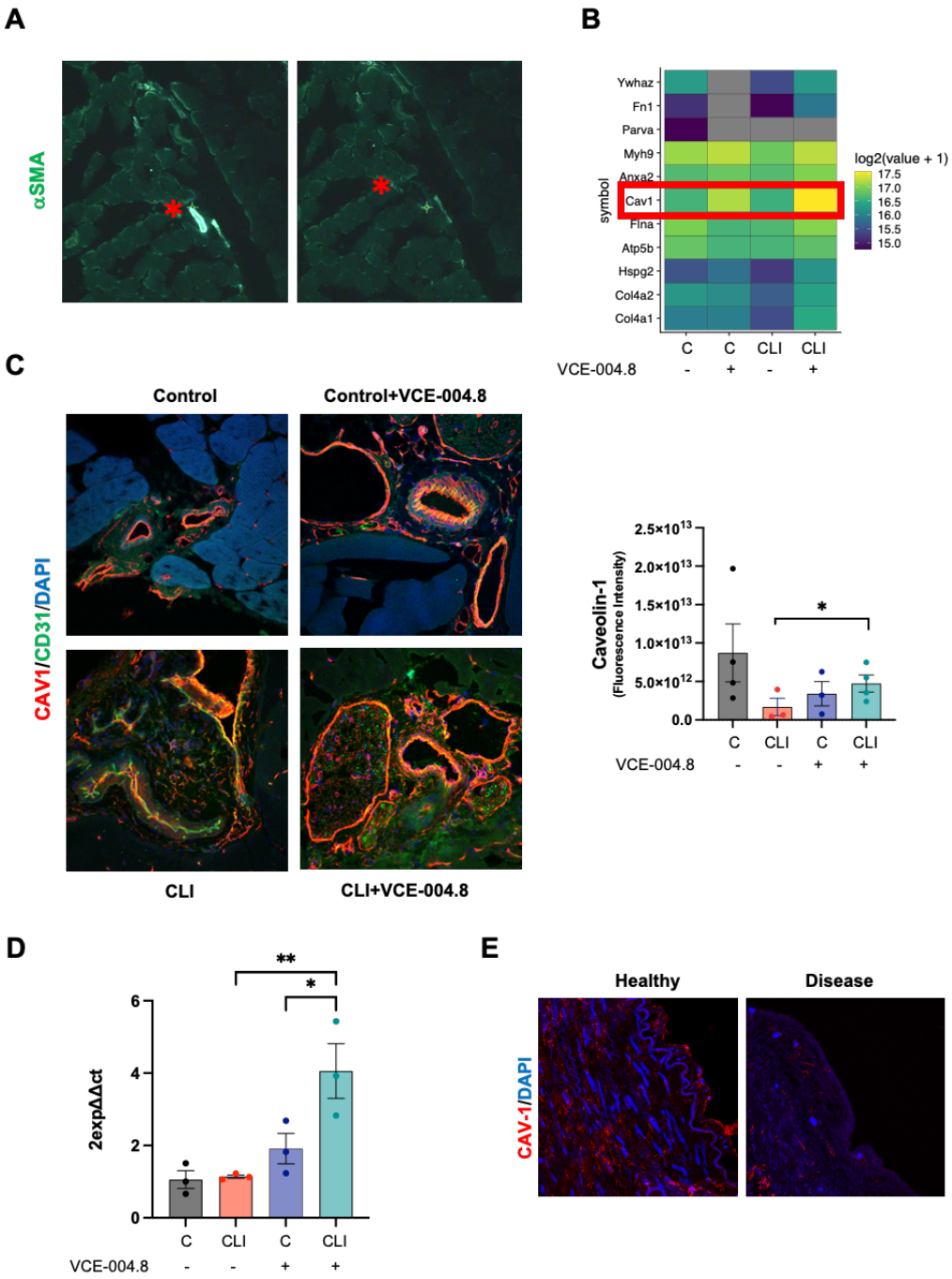
A
αSMA
B
Ywhaz
Fn1
Parva
Myh9
Anxa2
Cav1
Flna
Atp5b
Hspg2
Col4a2
Col4a1
symbol
log2(value + 1)
17.5
17.0
16.5
16.0
15.5
15.0
C C CLI CLI
VCE-004.8 - + - +
C
Control
Control+VCE-004.8
CAV1/CD31/DAPI
CLI
CLI+VCE-004.8
Caveolin-1
(Fluorescence Intensity)
2.5×10^13
2.0×10^13
1.5×10^13
1.0×10^13
5.0×10^12
0.0
*
C CLI C CLI
VCE-004.8 - - + +
D
**
*
2expΔΔct
6
4
2
0
C CLI C CLI
VCE-004.8 - - + +
E
Healthy
Disease
CAV-1/DAPI

Figure 8